Weierstraß-Institut

für Angewandte Analysis und Stochastik

im Forschungsverbund Berlin e. V.

Preprint ISSN 0946 – 8633

Self-compression of 120 fs pulses in a white-light filament

Jens Bethge[1], Günter Steinmeyer[1], Gero Stibenz[2], Peter Staudt[2],

Carsten Brée[3,1], Ayhan Demircan[3], Harald Redlin[4], Stefan Düsterer[4]

submitted: July 19, 2010

[1] Max Born Institute for Nonlinear Optics and Short Pulse Spectroscopy, Max-Born-Straße 2A, 12489 Berlin, Germany

[2] Angewandte Physik und Elektronik GmbH (APE), Plauener Straße 163-165, D-13053 Berlin, Germany

[3] Weierstrass Institute for Applied Analysis and Stochastics, Mohrenstraße 39, 10117 Berlin, Germany

[4] Deutsches Elektronen-Synchrotron (DESY), Notkestraße 85, 22607 Hamburg, Germnay

No. 1529

Berlin 2010

2010 *Mathematics Subject Classification.* Primary 78A60.

2008 *Physics and Astronomy Classification Scheme.* 42.65.-k, 52.38.Hb.

Key words and phrases. Nonlinear Schrödinger Equations, Optical self-focusing, Ultrashort pulse propagation.

We kindfully acknowledge financial support by the Deutsche Forschungsgemeinschaft, grants DE 1209/1-2 and STE 762/7-2.

Edited by
Weierstraß-Institut für Angewandte Analysis und Stochastik (WIAS)
Mohrenstraße 39
10117 Berlin
Germany

Fax: +49 30 2044975
E-Mail: preprint@wias-berlin.de
World Wide Web: http://www.wias-berlin.de/

Abstract

Self-compression of pulses with > 100 fs input pulse duration from a 10 Hz laser system is experimentally demonstrated, with a compression factor of 3.3 resulting in output pulse durations of 35 fs. This measurement substantially widens the range of applicability of this compression method, enabling self-compression of pulsed laser sources that neither exhibit extremely low pulse-to-pulse energy fluctuations nor a particularly clean beam profile. The experimental demonstration is numerically modeled, revealing the exact same mechanisms at work as at shorter input pulse duration. Additionally, the role of controlled beam clipping with an adjustable aperture is numerically substantiated.

1 Introduction

Immediately after its first description by Hauri *et al.*, femtosecond filamentation has found widespread application for compressing laser pulses with energies in the range from hundred microjoules up to several millijoules [1]. Compared to other pulse compression techniques, such as the hollow fiber compressor [2], self-guiding filaments are intriguing as they completely eliminate potential damage issues of a guiding structure. While early demonstrations of filament compression still required chirped mirrors for dispersion compensation[1], more recent demonstrations of filament compression achieved spectral broadening and dispersion compensation in the filament channel [3]. The self-compression of laser pulses further simplifies the generation of intense short laser pulses and increases the attractiveness of filament compression schemes.

Despite numerous experimental demonstrations of both, self-compression [3, 5, 4, 6, 8, 7, 9] and chirped-mirror based filament compression [1, 11, 13, 12], however, optimized filament compression is still a very challenging task as it can only successfully be exploited in a small parameter window at the verge of two competing collapse scenarios. While increasing intensity or gas pressure will enhance spectral broadening and thereby the potential shortness of a compressed pulse, such simple parameter scaling is ultimately limited by the break-up of the beam profile into multiple filaments [15, 14], as originally suggested by Bespalov and Talanov [16]. This spatial break-up is induced by an azimuthal modulational instability, seeded by initial spatial beam distortions. Additionally, a second break-up scenario can easily occur along the propagation axis, giving rise to temporal fragmentation of the pulse into an irregular train of two or more pulses [3, 17]. Ultimately, neither type of fragmentation, spatial or tempo-

ral, can be tolerated in applications of compressed pulses. Yet, optimum performance of the self-compression scheme is often found at the verge to instability.

The proximity to break-up scenarios becomes a problem when lasers with strong energy fluctuations are being used for self-compression. Consequently, most demonstrations of filament compression have nearly exclusively utilized kHz femtosecond amplifier systems with their comparatively weak pulse-to-pulse fluctuations. Given currently available pump power and cooling technology, such lasers are typically limited to about 5 mJ pulse energy. Compared to their few-Hertz counterparts, kHz lasers typically exhibit superior beam quality and input pulse durations below 100 fs, which is considered to delay multifilament and temporal break-up, respectively. Given that there is little alternatives for scaling pulse energies above 10 mJ, however, it is the few-Hertz class of lasers that could benefit most from filamentation as there are essentially no working schemes for pulse compression in this regime. In the following, we will demonstrate filament self-compression with a 10 Hz laser system that neither exhibits exceptional beam quality nor sub-100 fs pulse duration. We show that it is possible to exploit filament self-compression with such a laser and indicate a less stringent set of criteria that needs to be fulfilled.

2 Experimental setup

The experiments reported are performed with a commercial system consisting of a regenerative Ti:sapphire amplifier (Hidra-25 F, Coherent Inc.) in combination with a 2-pass booster amplifier system that delivers up to 25mJ pulses at a repetition rate of 10 Hz. The amplifier is pumped with a flash lamp pumped laser (Surelite II, Continuum Inc.). However, for our self-compression experiments only a 5 mJ fraction of this energy was used, which were further attenuated down to about 1 mJ by an iris. For a complete characterization of the laser pulses we use a spectral phase interferometry for direct electric-field reconstruction (SPIDER) [18]. For our measurements, we use commercial apparatus that employs asymmetric group velocity matching in a long nonlinear optical crystal, i.e., a variant that is also known as LX-SPIDER [19]. This technique enables reliable and immediate pulse characterization of the > 100 fs input pulses as well as of the compressed output pulses in the sub-40 fs regime. Like all other SPIDER techniques, LX-SPIDER measures the spectral phase of the pulses under test, allowing for reconstruction of temporal pulse profile and chirp with additional information on the spectrum of the pulses. Figures 1a and b show the measured spectral power density of the input pulses (red line) and the spectral phase from the LX-SPIDER measurements (red line). The resulting temporal profile of the pulse is indicated by the red line in Fig.1c. The profile of the input pulses exhibits only negligible deviations from the ideal profile of a bandwidth-limited pulse (dashed line) at negative delay positions, as shown as the green line in the same graph. Thus, the pulse duration of 115 fs cannot be significantly reduced without using nonlinear optical effects for expanding the bandwidth of the pulses.

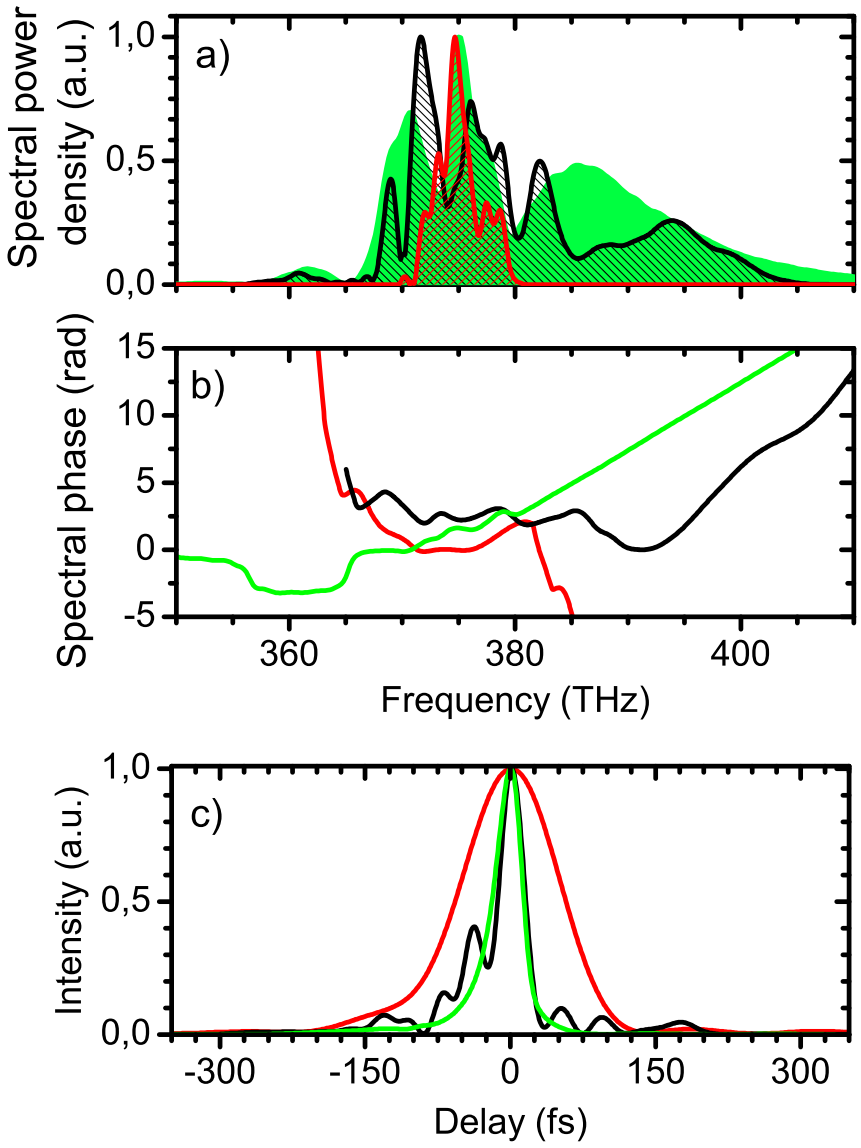

Figure 1: **a** Spectral power density of a representative input pulse (red line), a experimentally measured output pulse after filamentary propagation (black line), and a theoretically predicted output pulse (green line, see Sect. 4). **b** Spectral phases of measured input pulse, the output pulse, and the theoretically predicted output pulse. **c** The resulting temporal structure of the input pulse, the output pulse, and the calculated output pulse.

In our experiment, self-generated filamentation serves for spectral broadening. The filament is generated within a Brewster windowed gas cell as previously employed for various compression methods in the mJ-range [3, 1, 2]. The main advantage of such a cell over simply using atmospheric air [13] is the adjustability of the nonlinearity via the pressure and the gas fill, for which we used krypton at atmospheric pressure throughout. It should be noted that the unavoidable 0.5 mm thick silica windows of the cell have been discussed to have an important impact on pulse formation [20]. As our laser system delivers relatively long > 100 fs output pulses, we can replace the focusing mirror by a simple lens, avoiding potential issues with astigmatism, which allows for some simplification. This measure may also to some extent delay spatial break-up of the filament [21]. For the measurements reported in this paper, a lens with a focal length of $f = 75$ cm is used at a distance of 25 cm to the Brewster-oriented input window. This lens exhibits half of the focal length used in previous experiments on self-compression [3]. This rather tight focusing is a necessary compromise for a compact in-line set-up. Our set-up additionally contains three adjustable apertures before and after the focusing lens and after the gas cell. Adjusting the diameter of the first diaphragm clips the outer rim of the spatial beam profile and is particularly important for obtaining a spatially stable single filament. The second aperture is helpful for fine tuning of the beam profile and the pulse energy, providing an additional degree of freedom to produce a single filament and for preventing multifilamentation. The third aperture, finally, only serves to limit the amount of light entering the LX-SPIDER apparatus and to restrict the measurement to the core of the filament.

For the application of pulse self-compression, the used laser system is not ideal concerning several aspects. One apparent problem of high-pulse energy systems is deviation from an Gaussian beam profile, in particular small-scale inhomogeneities. An added problem is the poor pointing stability of such systems. Figure 2 shows the color-coded intensity beam profile of the laser, with lighter colors indicating higher energies. The beam profile shows an inhomogeneous mode structure with a vertical width of $\Delta Y = 25$ mm and a horizontal one of $\Delta X = 20$ mm. This profile exhibits several hot spots, which may compete in seeding independent filaments provided sufficient input energy. We measured a series of 1000 successive beam profiles and computed the center of gravity of each frame, as indicated by the red dots in Fig. 2. The rms spread of these dots amounts to 168 μm, i.e., is just 1 percent of the beam dimensions. For stabilizing the filament, we spatially filter the input beam with a diaphragm, rejecting all light outside a 1.5 mm diameter around the center of gravity. This portion of the beam also shows the weakest pulse-to-pulse energy fluctuations, amounting to about 10% rms for the 1000 recorded profiles. The remaining pulse energy amounts to about 1 mJ. The resulting beam is more stable in time and shows a much cleaner beam profile, which may further improve due to the self-cleaning effect during filamentary propagation [22].

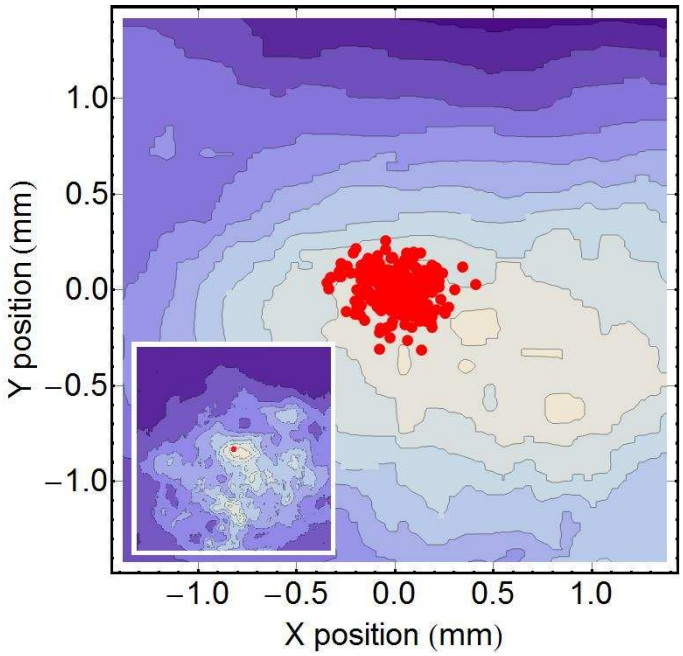

Figure 2: A characteristic beam profile of the laser, showing different hot spot areas and one prominent hotpot (lighter colors indicate higher energies). The red dots show the position of the center of gravity for 1000 successive pulses. The inset shows the whole beam profile with a diameter of about 1 inch.

3 Experimental results

Under the described experimental conditions inside the gas cell, we observe formation of a single filament that complies with the criteria in Ref. [23]. In particular, the filament exhibits a strongly ionized region at location of the classical focus, followed by a post-ionization regime. In kHz experiments both these zones are typically clearly distinguishable and exhibit a characteristic fluorescence and scattered white-light, respectively. In the current experimental setup, it is not possible to clearly measure the total length of the filament, since the intensity of the light scattered from the post-ionization channel is low, due to the low repetition rate of the used laser system. However, filament formation is evident from the beam profile after cell, indicating beam confinement over more than the Rayleigh length of the focal geometry employed here. Additionally, strong nonlinear interaction can be deduced from the output spectrum after the cell. By increasing the aperture diameter, i.e., also increasing pulse energy, one first observes a small amount of blue frequencies created in the clearly visible plasma flame forming at the linear focus of the beam. A further increase of pulse energy leads to a sudden appearance of a significant white-light spot in the far-field behind the gas cell, showing a different divergence behavior than the original beam. Still further increasing the energy, multiple filaments start to form, as indicated by two or more spots in the far field. In contrast to the behavior of the single filament these multiple filaments are not stable in position and show unpredictable dynamics. The broadest spectrum and best compression ratio have been observed for an energy slightly below the on-set of multiple filamentation, similar to the observations in Ref. [3].

Figures 1a and b show measured spectral amplitude and phase of the pulse after the filamentary propagation, respectively. The measured data is shown as a black curve, which is to be compared with numerically simulated data (green curves) that will be further discussed in the next section. The simulations are based on the experimental conditions of the input pulse (Gaussian pulse shape with $115\ \mathrm{fs}$ pulse duration, focused by an $\mathrm{f} = 75\ \mathrm{cm}$ lens). Inspecting the output spectrum shown in Fig. 1 (a, black line) and comparing it to the input pulse (red line), one finds prevalent spectral broadening towards blue frequencies ($380 - 405\ \mathrm{THz}$) by about $25\ \mathrm{THz}$. This is contrasted by a marginal $4\ \mathrm{THz}$ broadening towards the red. This asymmetric broadening is another indication for a strong influence of plasma effects in the broadening process. The characteristic asymmetry has been previously explained by self-steepening [24] and is typical for filament compression. Compared to the $\approx 8\,\mathrm{THz}$ width (FWHM) of the input spectrum, the spectrum from the filament encompasses a 4 to 5 times wider range. The Fourier-limited pulse duration of the filament output amounts to 22 fs, indicating a possible 4.7-fold temporal compression in the filament process.

The spectral phase as measured with the LX-SPIDER apparatus is plotted in Fig. 1 (b, black curve). The spectral phase is relatively flat up to 390 THz and starts to roll off in the extreme blue range of the newly generated spectral content. Numerical simulations indicate a similar behavior with a flat spectral phase in the central part of the spectrum, however starting to roll off some 10 THz lower than in the experiments.

Figure 1c shows the resulting temporal profile of the self-compressed pulse (red line). Comparing the pulse duration one finds a compression by a factor of 3.3 from 115 fs to 35 fs. The pulses were characterized after a third aperture, which is placed after the gas cell and which separates the filament light from light that was scattered into the reservoir region. This isolates the white-light core of the filament. The core has a highly improved spatial profile compared to the initial profile of the beam and is spatially stable, with an rms deviation of pulse energy of about 13 percent, an instability being only 3 percent higher than that of the input pulses.

4 Numerical simulations

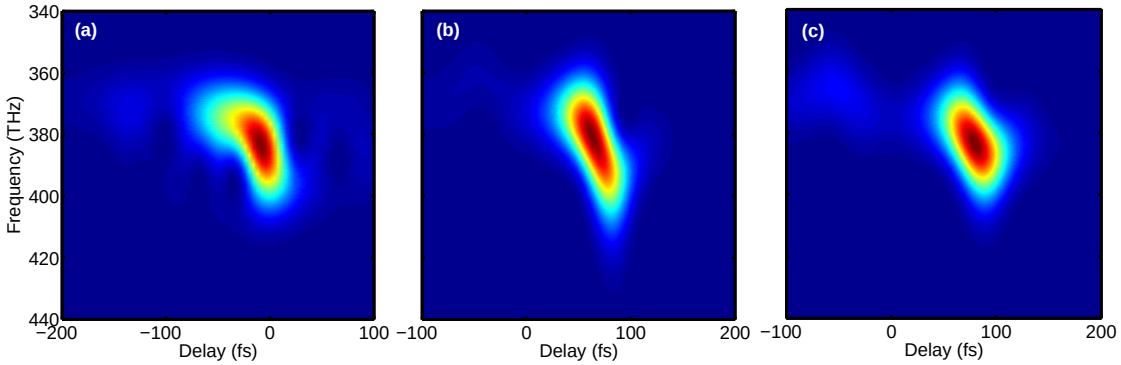

Figure 3: **a** XFROG trace reconstructed from experimental SPIDER data **b** XFROG spectrogram of an apertured output pulse, numerically simulated, with initial temporal profile taken from experiment. **c** Corresponding XFROG spectrogram for unapertured input pulse.

Filamentary self-compression has been previously discussed as mainly resulting from spatial effects [1, 5, 17, 25]. As the pulse is spatially confined in traditional compression schemes [26], energy transport can only occur along the longitudinal axis. Filament scenarios do not obey any such constraints on the beam radius, and energy transport in radial direction may also occur. In particular, this may give rise to a time-dependent beam diameter along the pulse. Such spatial mechanisms have been recently confirmed as the dominant mechanism behind filament self-compression of sub-50 fs input pulses. This spatial compression mechanism is in contrast to some earlier explanation of an observed self-compression of longer pulses in the 150 fs regime [27]. Koprinkov et al. explained their findings by spatio-temporal soliton formation, an explanation that neglects plasma formation and the azimuthal modulational instability [16], and that was subsequently questioned by others [28]. This may serve as a motivation for our numerical studies, which we conducted to see whether the now widely recognized explanation for self-compression also applies for longer pulse durations.

For this purpose, we performed numerical simulations of the generalized Nonlinear Schrödinger Equation [5], modeling filamentary propagation of the envelope of the light electric field. To match experimental conditions, special emphasis is put on proper modeling of initial conditions, for which we used experimentally measured SPIDER data. In the view of its important role in the experiments, we included the second aperture in our numerical modeling. The envelope of the initial electric field distribution used in the numerics is described by

$$\begin{aligned} \mathscr{E}(r,t) &= \sqrt{I_{\max}} \exp\left(-2\frac{r^2}{w_0^2} - 2\frac{r^{16}}{d_{\mathrm{ap}}^{16}}\right) \\ &\times \int_{-\infty}^{\infty} d\omega \exp\left(i\frac{r^2}{2k(\omega)f} + i\phi(\omega) + i\omega t\right)\sqrt{\tilde{I}(\omega)}. \end{aligned} \tag{1}$$

Here, the initial beam waist is given by $w_0 = 2.5\,\mathrm{mm}$, a value which appears reasonable for the hot spot selected by the first aperture. $I(\omega)$ and $\phi(\omega)$ are the measured spectrum and spectral phase of the input pulse, respectively. $I_{\max}$ is the peak temporal intensity, assuming a proper normalization of $\tilde{I}(\omega)$. The peak intensity of the input pulse can then be estimated according to

$$I_{\max} \approx \frac{2E_{\mathrm{in}}}{\pi w_0^2 \int dt I(t)}, \tag{2}$$

where $I(t)$ is the temporal intensity profile reconstructed from measured SPIDER data, normalized to unity. The diameter of the second aperture is given by d_{ap}, and $E_{\mathrm{in}} \approx 1\,\mathrm{mJ}$ is the laser pulse energy transmitted through the first aperture. A super-Gaussian was used to model the aperture, to avoid numerical artifacts. As our numerical model includes space-time focusing effects that arise because different frequency components diffract into different cone angles we utilized a frequency-dependent factor $\exp(ir^2/2k(\omega)f)$ with $f = 75\,\mathrm{cm}$ in the Fourier-domain for proper modeling of the lens [29]. Here $k(\omega) = n(\omega)\omega/c$ is the wave number in krypton, with dispersion modeled according to Ref. [30].

We analyze the propagation of the apertured input pulse with $d_{\mathrm{ap}} = 5\,\mathrm{mm}$, where the experimental SPIDER data of the $115\,\mathrm{fs}$ pulse is used for the initial temporal profile. The chosen aperture size amounts to a transmitted energy through the second aperture of $\approx 0.8\,\mathrm{mJ}$. In fact, it turns out that the pulse duration of the numerically simulated, self-compressed pulse (34 fs) matches that of the measured pulse within experimental precision, as is obvious from the representation of the on-axis temporal intensity profile shown in Fig. 1.

The simulations allow for a calculation of XFROG spectrograms, which are a proven tool to analyze the spatio-temporal structure in various supercontinuum scenarios. These spectrograms can also be computed from experimental data, provided that a complete characterization method as SPIDER was used. Such spectrograms are shown in Fig. 3, with an excellent quantitative and qualitative agreement of experimental and simulated spectrograms. These spectrograms indicate a characteristic

inverse Γ shape which emerges due to asymmetric spectral broadening in the self-steepened trailing edge of the pulse. This feature has independently been confirmed in experiments and numerical simulations [5] for shorter pulses and clearly confirm that one and the same mechanism is at work in both pulse duration regimes. This analysis also rules out spatio-temporal solitons [27] of any kind, as these would to lead to rather featureless round or elliptic spectrogram representations. The evolution of the on-axis temporal profiles leading to the charactereristic Γ-shaped spectrograms can be visualized by the color-coded representation of the evolution of the on-axis temporal intensity profile along the propagation direction z shown in Fig. 4a. This shows temporal break-up in the vicinity of the focal region, followed by a subsequent isolation of a self-compressed trailing subpulse experiencing further temporal compression in a weakly ionized channel for $z > 0.8\,\mathrm{m}$. This behavior clearly confirms that the self-compression evolves according to the spatially dominated self-pinching mechanism of [25]. In fact, the remnants of the suppressed leading subpulse can be observed both in the measured and simulated XFROG traces Figs. 3a and b.

To demonstrate the impact of the aperture, we performed a simulation with unchanged initial conditions, however neglecting the aperture ($d_{\mathrm{ap}} = \infty$). In this case, the full $1\,\mathrm{mJ}$ energy of the unapertured input pulse is available for filamentary propagation. The spectrogram representation of the emerging output pulse shown in Fig. 3c reveals that the pulse has experienced less spectral broadening in the trailing edge as compared to the apertured pulse. Also, we observe an increased pulse duration (FWHM) of $\approx 36\,\mathrm{fs}$. Thus, we observe that aperturing the input pulse enhances spectral broadening. Indeed, a comparison of the evolution of apertured and unapertured input pulses in the numerical simulations shown in Figs. 4a and b and the evolution of the peak electron densities for both cases as shown in Fig. 4c reveal the origins of this surprising effect. In fact, the dynamical behaviour for the unapertured case Fig. 4b agrees qualitatively with the evolution of the apertured pulse Fig. 4a, yet with reduced longitudinal dimension of the nonlinear focus and a reduction of the intensity in the weakly ionized channel, as is obvious from comparing the evolution of the peak electron densities for the two cases as shown in Fig. 4c. We thus observe that this reduces the efficiency of spectral broadening for the unapertured case and the given aperture and input pulse parameters. Finally, the enhanced nonlinearity encountered by the apertured input pulse increases its spectral broadening and gives rise to a reduced pulse duration for the output pulse.

In conclusion, our results clearly emphasize the importance of proper modeling of initial conditions, leading to a remarkable quantitative agreement between experimentally measured pulse durations and numerical simulations. The simulations correctly predict an approximate fourfold temporal compression of the initial $115\,\mathrm{fs}$ input pulse as well as the characteristic Γ shaped XFROG traces.

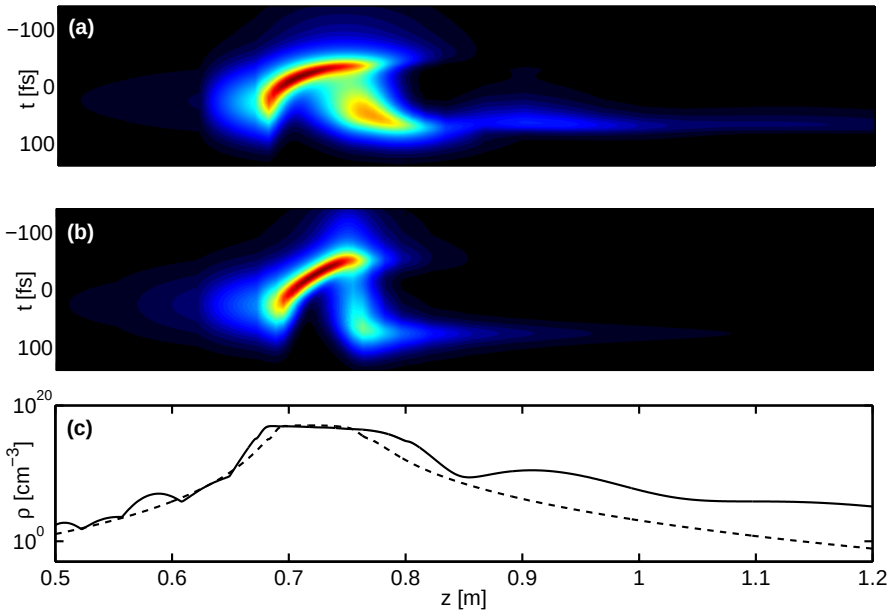

Figure 4: **a** Evolution of on-axis temporal profile, apertured input pulse. **b** Evolution of on-axis temporal profile, unapertured input pulse. **c** Evolution of peak electron density along z for apertured (dashed line) and unapertured (solid line) input pulses.

5 Discussion

As the experiments clearly reveal, filament self-compression can be exploited even with laser systems that appear to be prone to induce either spatial or temporal breakup in the compression process. In particular, at first sight, it seems surprising that a beam profile with several hot-spots (cf. Fig. 2) does not automatically and unavoidably induce multiple filamentation. Let us recall, however, that filament formation is described by a deterministic set of equations, which lead to the same spatial and temporal characteristics when the same input parameters are fed into the system. While the presence of hot spots in the beam profile will certainly prefer initialization of filaments at these locations, however, only strong pulse-to-pulse fluctuations of either beam profile or temporal pulse shape are expected to turn out prohibitive for meeting the small parameter window where self-compression can take place. Therefore, low pulse-to-pulse fluctuations are expected to be the key parameter for successful self-compression schemes at few-Hertz repetition rate. In fact, such conditions could not be met in an earlier set of experiments with a 10 Hz laser, cf. Sect. II in Ref. [5]. In these experiments, single filamentation and a short compressed pulse could only be seen for a small percentage of the laser shots. In addition, our numerical analysis clarifies the role of aperturing the input pulses. This measure does not only help to stabilize the filament, preventing spatial breakup and multiple filamentation, but it also increases the longitudinal extension of the nonlinear interaction region in the vicinity

of the focus, giving rise to spectrally broader and temporally shorter output pulses.

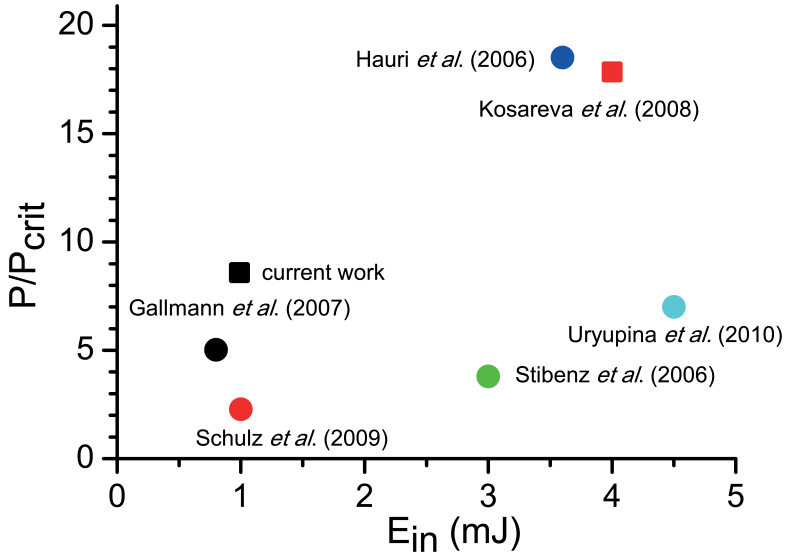

Figure 5: Comparison of power levels required for meeting the condition for self-compression. Ordinate is normalized to critical power P_{cr}. Circles refer to kHz repetition rate experiments (Hauri *et al.* [4], Gallmann *et al.* [8], Stibenz *et al.* [3], Schulz *et al.* [7] and Uryupina *et al.*[10]), squares to 10 Hz systems (Kosareva *et al.* [9] and current work).

For further analysis of our results, we have compiled a comparison of input peak powers required for meeting the conditions for filament self-compression in various experiments, see Fig. 5. This data comprises experiments at 10 Hz and kHz repetition rates as well as in different noble gases. Quite clearly, the experiments at 3 mJ input pulse energy or below used input powers that were only about a factor 3 above the critical power $P = \lambda^2/2\pi n_2$. All experiments at higher pulse energies, however, also reported significantly higher values up to 20 critical input powers, which is somewhat surprising as multiple filamentation appears hard to avoid at such elevated power levels. In our current experiments, using krypton as the medium we could reach self-compression at only 8 critical powers, which is significantly lower than in the only other 10 Hz experiment published so far. This may pave a way towards further increase of pulse energies without suffering from spatial break-up.

6 Conclusion

Among the different criteria that have been brought up for deciding the suitability of an amplifier system for self-compression, our experiments clearly indicate a surpris-

ingly low importance of pulse duration and spatial beam quality. Starting with pulses of 115 fs duration, a compression factor larger than 3 could be obtained. This extends applicability of self-compression schemes to durations that are about 3 times as long as used in most previous experiments. We numerical verified the the role of the input aperture and demonstrated its impoartance for effectiveness ot the self-compression mechanism. However, our experiments also emphasize the importance of small pulse-to-pulse fluctuations for successful application of this compression method. Obviously, this criterion does not only include fluctuations of the pulse energy but also requires small pulse-to-pulse variations in beam profile and temporal structure of the pulse, which are, however, difficult to monitor. Given that these criteria can be fulfilled at higher pulse energies and given that the nonlinearity is adapted by suitable choice of medium and pressure, we do not see any systematic limitation for application of self-compression schemes. Using gases with lower nonlinearity, self-compression may therefore open up a perspective at pulse energies where practically no active compression schemes are available to date, allowing for the concentration of energy to a volume encompassing only a few wavelengths laterally as well as longitudinally.

References

[1] C.P. Hauri, W. Kornelis, F.W. Helbing, A. Heinrich, A. Couairon, A. Mysyrowicz, J. Biegert, and U. Keller, Appl. Phys. B **79**, 673–677 (2004).

[2] M. Nisoli, S. De Silvestri, O. Svelto, R. Szipőcs, K. Ferencz, C. Spielmann, S. Sartania, and F. Krausz, Opt. Lett. **22**, 522–524 (1997).

[3] G. Stibenz, N. Zhavoronkov, and G. Steinmeyer, Opt. Lett. **31**, 274–276 (2006).

[4] C. P. Hauri, A. Trisorio, M. Merano, G. Rey, R. B. Lopez-Martens, and G. Mourou, Appl. Phys. Lett. **89**, 151125 (2006).

[5] S. Skupin, G. Stibenz, L. Bergé, F. Lederer, T. Sokollik, M. Schnürer, N. Zhavoronkov, and G. Steinmeyer, Phys. Rev. E **74**, 056604 (2006).

[6] C. P. Hauri, R. B. Lopez-Martens, C. I. Blaga, K. D. Schultz, J. Cryan, R. Chirla, P. Colosimo, G. Doumy, A. M. March, C. Roedig, E. Sistrunk, J. Tate, J. Wheeler, L. R. DiMauro, and E. P. Power, Opt. Lett. **32**, 868–870 (2007).

[7] E. Schulz, T. Binhammer, D. S. Steingrube, S. Rausch, M. Kovacev and U. Morgner, Appl. Phys. B **95**, 269–272 (2009).

[8] L. Gallmann, T. Pfeifer, P.M. Nagel, M.J. Abel, D.M. Neumark, S.R. Leone, Appl. Phys. B **86**, 561–566 (2007).

[9] O. G. Kosareva, N. A. Panov, D. S. Uryupina, M. V. Kurilova, A. V. Mazhorova, A. B. Savelev, R. V. Volkov, V. P. Kandidov, and S. L. Chin, Appl. Phys. B **91**, 35–43 (2008).

[10] D. Uryupina, M. Kurilova, A. Mazhorova, N. Panov, R. Volkov, S. Gorgutsa, O. Kosareva, A. Savel'ev, and S. L. Chin, J. Opt. Soc. Am. B **27**, 667–674 (2010).

[11] A. Zaïr, A. Guandalini, F. Schapper, M. Holler, J. Biegert, L. Gallmann, A. Couairon, M. Franco, A. Mysyrowicz, and U. Keller, Opt. Express **15**, 5394–5404 (2007).

[12] O. Varela, A. Zaïr, J. San Román, B. Alonso, I. J. Sola, C. Prieto, and L. Roso, Opt. Express **17**, 3630–3639 (2009).

[13] B. E. Schmidt, W. Unrau, A. Mirabal, S. Li, M. Krenz, L. Wöste, and T. Siebert, Opt. Express **16**, 18910–18921 (2008).

[14] S. Tzortzakis, L. Bergé, A. Couairon, M. Franco, B. Prade, and A. Mysyrowicz, Phys. Rev. Lett. **86**, 5470–5473 (2001).

[15] L. Bergé, S. Skupin, F. Lederer, G. Meéjean, J. Yu, J. Kasparian, E. Salmon, J. P. Wolf, M. Rodriguez, L. Wöste, R. Bourayou, and R. Sauerbrey, Phys. Rev. Lett. **92**, 225002 (2004).

[16] V. I. Bespalov and V. I. Talanov, JETP Lett. **3**, 307–310 (1966).

[17] M. Mlejnek, E. M. Wright, and J. V. Moloney, Opt. Lett. **23**, 382-384 (1997).

[18] C. Iaconis and I. A. Walmsley, IEEE J. Quantum Electron. **35**, 501–509 (1999).

[19] A. S. Radunsky, E. M. K. Williams, I. A. Walmsley, P. Wasylczyk, W. Wasilewski, A. B. U'Ren, M. E. Anderson, Opt. Lett. **31**, 1008–1010 (2006).

[20] L. Bergé, S. Skupin, and G. Steinmeyer, Phys. Rev. Lett. **101**, 213901 (2008).

[21] G. Fibich, I. S. Eisenmann, B. Ilan, A. Zigler, Opt. Lett. **29**, 1772–1774 (2004).

[22] W. W. Liu and S. L. Chin, Phys. Rev. A **76**, 013826 (2007).

[23] S. L. Chin, Y. Chen, O. Kosareva, V. P. Kandidov, F. Théberge, Laser Phys. **18**, 962–964 (2008).

[24] A. L. Gaeta, Phys. Rev. Lett. **84**, 3582–3585 (2000).

[25] C. Brée, A. Demircan, S. Skupin, L. Bergé, and G. Steinmeyer, Opt. Express **17**, 16429–16435 (2009)

[26] R. L. Fork, O. E. Martinez, and J. P. Gordon, Optics Letters. **9**, 150–152 (1984).

[27] I. G. Koprinkov, A. Suda, P. Wang, and K. Midorikawa, Phys. Rev. Lett. **84**, 3847–3850 (2000).

[28] A. L. Gaeta and F. Wise, Phys. Rev. Lett. **87**, 229401 (2001).

[29] L. Bergé, S. Skupin, and G. Steinmeyer, Phys. Rev. A **79**, 033838 (2009).

[30] A. Dalgarno and A. E. Kingston, Proc. Roy. Soc. A **259**, 424–431 (1960).